Assimilation of HF radar-derived surface currents on tidal-timescales

G Gopalakrishnan, Climate, Atmospheric Science and Physical Oceanography, Scripps Institution of Oceanography
AF Blumberg, Center for Maritime Systems, Stevens Institute of Technology

A surface current observation system based on high-frequency (HF) radar has been developed for Raritan Bay and the coastal waters of New York and New Jersey. An HF radar network provides synoptic surface current maps in near-real-time that can be optimally combined with ocean circulation models using data assimilation (DA) framework to obtain the best possible estimate of a three-dimensional ocean state. A nudging or Newtonian damping scheme has been developed to assimilate HF radar data into an estuarine and coastal ocean circulation model. This model, with an extensive embedded real-time observational network, is called the New York Harbour Observing and Prediction System (NYHOPS). A nudging parameter is introduced into the equations of motion which affects the model dynamics. The data is imparted to neighbouring (three-dimensional) grid points via model dynamics. The impact of HF radar DA is analysed by computing the DA skill score (DA_{skill}) based on the mean-square-error (*mse*). The DA_{skill} is computed by comparing non-assimilated and assimilated model solutions with *in-situ* observations of three-dimensional currents, temperature and salinity, which have not been included in the assimilation. A positive DA_{skill} (0~1) represents an improvement in the model performance by assimilation. HF radar data covering Raritan Bay and the New York Bight (NYB) Apex were assimilated into the NYHOPS model in the model hindcast cycle (–24h to 0h) on a daily forecast basis for a period of 40 days. The DA_{skill} is assessed with respect to the NYHOPS model hindcasts (daily model solutions from –24h to 0h) as well as the first day forecasts (daily model solutions from 0h to 24h). HF radar DA improved the NYHOPS model performance during both the hindcast and forecast periods. The model skill metrics for the near-surface layers in the inner-NJ shelf region shows a hindcast DA_{skill} of 24% (14%) and forecast DA_{skill} of 18% (7%) for horizontal velocities *u: east-west component* (*v: north-south component*), and a hindcast DA_{skill} of 33% (38%) and forecast DA_{skill} of 25% (30%) for temperature (salinity). The nudging scheme is robust and efficient for the HF radar DA into the NYHOPS operational forecast model. The NYHOPS-HF radar DA system is capable of importing in the observations and produce useful hindcasts/forecasts with minimum computational expense.

AUTHORS' BIOGRAPHIES

Ganesh Gopalakrishnan holds a PhD in ocean engineering and is a post-doctoral researcher at Scripps Institution of Oceanography. His research interests are mainly focused on state estimation techniques, forecasting, and predictability of the ocean state.

Alan F Blumberg is George Meade Bond Professor of Ocean Engineering at Stevens Institute of Technology. He is the recipient of the 2001 Karl Emil Hilgard Hydraulic Prize and the 2007 IMarEST Denny Medal. He received his training in ocean physics at Johns Hopkins University and Princeton University.

INTRODUCTION

Today's numerical ocean models are capable of simulating three-dimensional (3D) ocean circulation over a wide range of scales: from regional estuarine, coastal ocean circulation to global ocean circulation. The dynamic seastate simulated by these models critically depends on the model boundary conditions, as well as the model's capability to resolve the water parameters, both spatially and temporally. Research and development in the field of instrumentation and technology over the last three decades has substantially improved coastal ocean observation systems. These advanced systems provide enormous amounts of ocean measurements in real-time, addressing the 'scarcity' of observational data in oceanography. The increasingly available ocean observational data are appropriate for 'data assimilation', where observational data are combined with a numerical model to obtain the best possible representation of the ocean state, which is better than could be obtained using just the numerical model or the observational data alone.[1]

The development of land-based HF radar systems over the last decade has provided a unique shore-based ocean observation platform that is capable of measuring ocean surface currents. With the expanding network of HF radars providing synoptic surface current maps in near-real-time, more and more surface-current data assimilation (DA) efforts have been focused on coastal regions. Earlier HF radar DA studies were more directed towards the low frequency circulation patterns, in which the higher frequency tidal signals were eliminated by low-pass filtering of the HF radar data prior to assimilating into the numerical ocean models. In some of the studies, the tidal forcing and surface heat fluxes were not considered in the ocean models.

In one of the earlier DA studies using HF radar data for Monterey Bay, California[2] a pseudo-shearing stress, defined by the difference between the model surface current and HF radar data, was used to correct the model wind forcing. Another study[3] reported HF radar surface current assimilation into a realistic coastal model for the Norwegian coast using an optimal interpolation (OI) method. An HF radar DA study for the Oregon coast[4] used a sequential OI scheme based on a physical-space statistical analysis system (PSAS) and a time-distributed averaging procedure (TDAP). A representer-based four-dimensional variational method (4D-VAR)[5] was used[6] to assimilate HF radar data into a simplified ocean model. Others[7] have assimilated HF radar data using a PSAS scheme based on data-dependent velocity covariance functions in Monterey Bay, in which the near-surface model currents were corrected and projected down into the water column based on physical arguments of energy conservation and Ekman theory. Assimilation of HF radar data using a melding/nudging approach has been reported[8] for the New Jersey inner-shelf. Another paper[9] reported assimilated HF radar surface currents in the West Florida shelf using an ensemble-based error covariance method. And a further paper[10] reported a three-dimensional variational assimilation (3D-VAR) of HF radar data in the Southern California on an operational basis. A 4D-VAR method has been used[11] to assimilate HF radar data in the San Diego coastal region. Recently, authors[12] reported assimilation of HF radar-derived radial/total surface currents using PSAS scheme for Monterey Bay, in which low-pass filtered (unfiltered) HF radar data were assimilated into non-tidal (tidal) ocean models.

The goal of this study is to develop a near-real-time HF radar data assimilation method for the New York Harbour Observing and Prediction System (NYHOPS) operational forecast model that resolves tidal frequency variability. In the present work, half hourly (~30 min) HF radar measured surface currents were assimilated into the primitive equation coastal ocean model (NYHOPS) using a cost-effective nudging assimilation scheme which resolves the tidal variability. This assimilation/forecast system for the urban estuaries of the New York/New Jersey (NY/NJ) Harbour and the NY Bight (NYB), incorporates tidal forcing, along with the forcing from the open ocean, surface meteorology, and freshwater inflows.

OCEAN OBSERVATIONS

HF radar observations

Over the last couple of decades, HF radar has emerged as one of the important components of the ocean observing system. The HF radar system works on the principle of radio wave backscatter by ocean surface gravity waves in the frequency band 3 ~ 30MHz, and is capable of mapping near-surface ocean currents over a spatial range of about 200km, depending upon the transmitting frequency.[13,14,15,16]

An HF radar network based on the Coastal Ocean Dynamics Application Radar (CODAR) system has been established in the NY/NJ Harbour waters and the NY Bight Apex. CODAR is a unique HF radar system consisting of a single pole transmitter antenna, and a compact and collocated three-element receiver antenna.[13] It works on a direction finding (DF) algorithm patented as multiple signal classification (MUSIC).[17] The HF radar network employed in the present study consists of four monostatic standard-range CODAR seasonde systems, located at Sandy Hook, NJ (HOSR: owned and operated by Rutgers University (RU)); Breezy Point, NY (BRZY: owned and operated by RU); Bayshore Water Front Park, NJ (BSWP: mobile system, owned and operated by National Ocean Atmospheric Administration (NOAA)); and on the south shore of Staten Island, NY (SILD: owned and operated by Stevens Institute of Technology (SIT)). The HF radar sites and the present study domain are shown in Fig 1.

HF radar systems work on the underlying assumptions of linear wave theory and deep water conditions. A single HF radar site measures only the radial component of the surface current, in which the Bragg scattering is predominant. HF radar systems measure the radial component of the surface current with respect to spatial domain defined by a polar coordinate system. The spatial domain is divided into annular bins called range cells (~1.5km, for standard-range CODAR seasonde) extending circularly from the HF radar site as the origin, and the azimuth ranges from 0° ~ 360°, incremented at every 5°. The total vector field of the surface currents is computed by combining the radial vectors measured by individual HF radar sites. This computation of the total vector field from the radial vectors follows a method of least squares suggested by[18]. A minimum of two or more radial vectors measured by the spatially separated HF radar sites, with at least one radial vector from each of the two different HF radar sites are com-

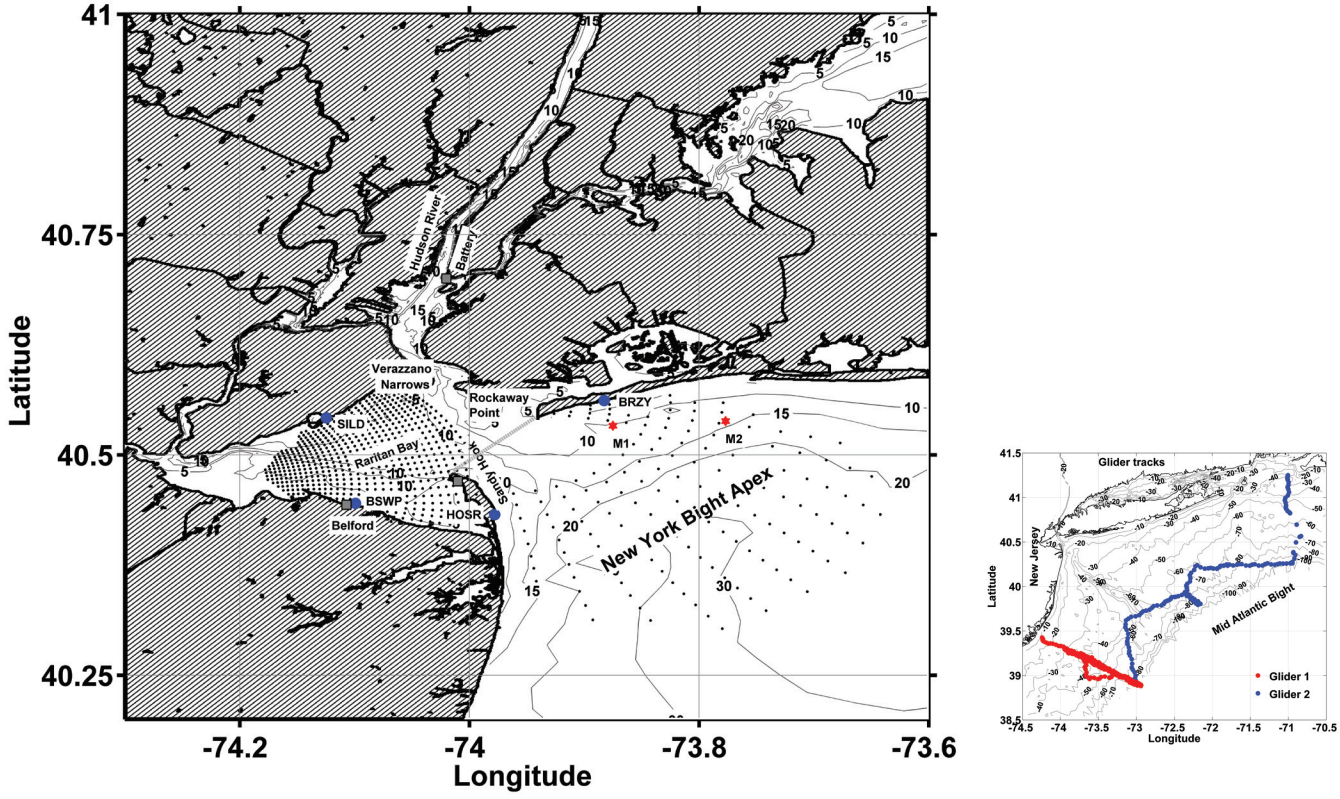

Fig 1: Location map showing the present study domain. Blue circles indicate HF radar stations, red star indicates ADCP mooring locations, and grey squares indicate fixed-sensor locations, dashed grey line indicates the Sandy Hook-Rockaway Point (SHRP) transact. HF radar data footprint is shown by black dots. Contour lines indicate the water depths in metres, only HF radar data points with temporal data coverage greater than 50% were used in this study. The trajectories of the glider data (G1 and G2) used for the model skill assessment is shown in the sub-figure

bined to obtain the total surface current field. Surface currents measured using HF radar are near-surface depth averaged (d ~ 0.5m, for standard-range CODAR seasonde) and the depth of influence is a function of the transmitting frequency of the HF radar system.[19] A detailed description of the HF radar network used in this study has been published,[20] which reports the surface current circulation in Raritan Bay and the NYB Apex measured using HF radar systems.

In the present study, radial vector fields generated by the four HF radar sites every 30min were combined with respect to a pre-defined surface grid using the method of least squares to generate the total vector field. The NYHOPS model horizontal grid was used as the pre-defined surface grid for the total vector field computation. The HF radar network used in the present study provided good coverage of surface currents in the NY Harbour, Raritan Bay, and the NYB Apex.

One of the quality control measures used in the HF radar total vector processing is the geometric dilution of precision (GDOP), which is defined as the spatial uncertainty associated with geometric combination of the radial vectors.[21,16] The GDOP uncertainty increases with the distance from the HF radar stations and reaches a maximum along the periphery of the HF radar data footprint, and along the baseline (line connecting the HF radar stations). In order to improve the HF radar data quality, the present study used a GDOP uncertainty threshold value of less than 1.5cm s^{-1}, and the maximum radial and total current magnitudes were limited to 1.5m s^{-1}. Another quality control measure used in the HF radar total vector processing is the temporal data coverage threshold, where only HF radar data with a temporal data coverage threshold value of greater than 50% were used in this study. The HF radar data footprint for the period of Jan–April 2007 and the bathymetric contours is shown in Fig 1.

ADCP observations

Acoustic Doppler Current Profiler (ADCP) observations in the NYB Apex were used to perform the DA_{skill} analysis in this study. The ADCPs (M1 and M2) were deployed and maintained by Rutgers University for the period 22 February 2007–27 April 2007, and were located in the vicinity of the Breezy Point (BRZY) HF radar station (located in Fig 1). The ADCPs provided u (east-west) and v (north-south) velocity components in 0.5m vertical bins and were hourly averaged. The M1 ADCP was deployed at a mean water depth of 12.3m from the surface (~ at third range-cell from BRZY HF radar station) at a radial distance of ~3.25km from the Breezy Point (BRZY) HF radar station. The M2 ADCP was deployed at a mean water depth of 16.7m from the surface (~ at seventh range-cell from BRZY HF radar station) at a radial distance of ~9.5km from the Breezy Point (BRZY) HF radar station. The ADCPs failed to provide a reliable dataset in the near-surface layers (~ 1.2m from the surface for M1 ADCP and ~6.2m from the surface for M2 ADRCP).

Glider based observations

Temperature (T) and Salinity (S) profiles from gliders in the NJ shelf region were used for the DA_{skill} analysis in this study. The gliders (G1 and G2) were deployed and maintained by

Rutgers University for March 2007, with their trajectories located in the NJ shelf region (Fig 1). The glider G1 flight (7 March 2007–3 April 2007) was across the NJ shelf with its trajectory extending from the inner-NJ shelf at Great Bay, south of NJ coastal ocean, to the outer-NJ shelf up to a depth of 100m. The glider G2 flight (13 March 2007–6 April 2007) was along the mid-NJ shelf region, with its trajectory extending from the Great Bay, south of NJ coastal ocean, to the Nantucket Islands, Massachusetts.

Fixed-sensor based observations

Moored temperature (*T*) observations in the NYHOPS domain were used for the DA_{skill} analysis in this study. Moored hourly surface and bottom temperature records were obtained from the National Ocean Service (NOS stations: The Battery (BATN6) and Sandy Hook (SDHN4)), Stevens Institute of Technology (SIT station: Belford (STBLD4)), and Rutgers University (ADCP moorings: M1 and M2) (Fig 1).

MODELLING BACKGROUND

NYHOPS (http://stevens.edu/maritimeforecast/) is an estuarine and coastal ocean forecast system based on an extensive real-time observational network of distributed sensors[22] which has been operational since the beginning of 2004. The system is designed to represent the water parameters, weather and environmental conditions of the NY/NJ Harbour Estuary, Raritan Bay, Long Island Sound, NY Bight, and the NJ coastal ocean in real-time, and to forecast the conditions in near and long-term.

The NYHOPS forecast model is a three-dimensional, time-dependent hydrodynamic model, based on the estuarine coastal and ocean model (ECOM), a direct descendant of the Princeton Ocean Model (POM).[23] This numerical model is based on an 'Arakawa-C' grid, and solves a coupled system of differential, prognostic equations describing the conservation of mass, momentum, heat, and salt. The model is based on orthogonal curvilinear co-ordinate system in the horizontal plane and σ co-ordinate system in the vertical plane. The vertical eddy viscosity coefficients were calculated using the Mellor-Yamada level 2.5 turbulence closure scheme[24] with subsequent modifications.[25,26] The model uses the shear-dependent Smagorinsky formulation[27] for the calculation of horizontal eddy viscosity, and a spatially varying bottom friction coefficient was employed in the present study.

The model recognises both the faster, barotropic external waves and the slower, baroclinic internal waves, and solves the corresponding barotropic and baroclinic equations with different time-steps using a mode-splitting technique. The external barotropic mode assumes homogeneous temperature and salinity and uses a computational time step of 1 second. The internal baroclinic mode employs stratification and uses a computational time step of 10 seconds. The high-resolution model domain consists of 147x452 (I x J) curvilinear segments in the horizontal plane, and 11 vertical σ levels. The model domain encompasses the entire NY/NJ Harbour Estuary, Long Island Sound, and the NJ and Long Island coastal ocean (Fig 2). The model domain includes the tidal Hudson River up to the federal dam at Troy, NY, at its northern boundary. The open ocean boundary of the model domain is bound to the: (a) southeast, at the continental shelf to depths lesser than the 200m isobath, (b) southwest, by a line extending from coastal Maryland south of Delaware Bay, and (c) east, to a cross-shelf line extending southward

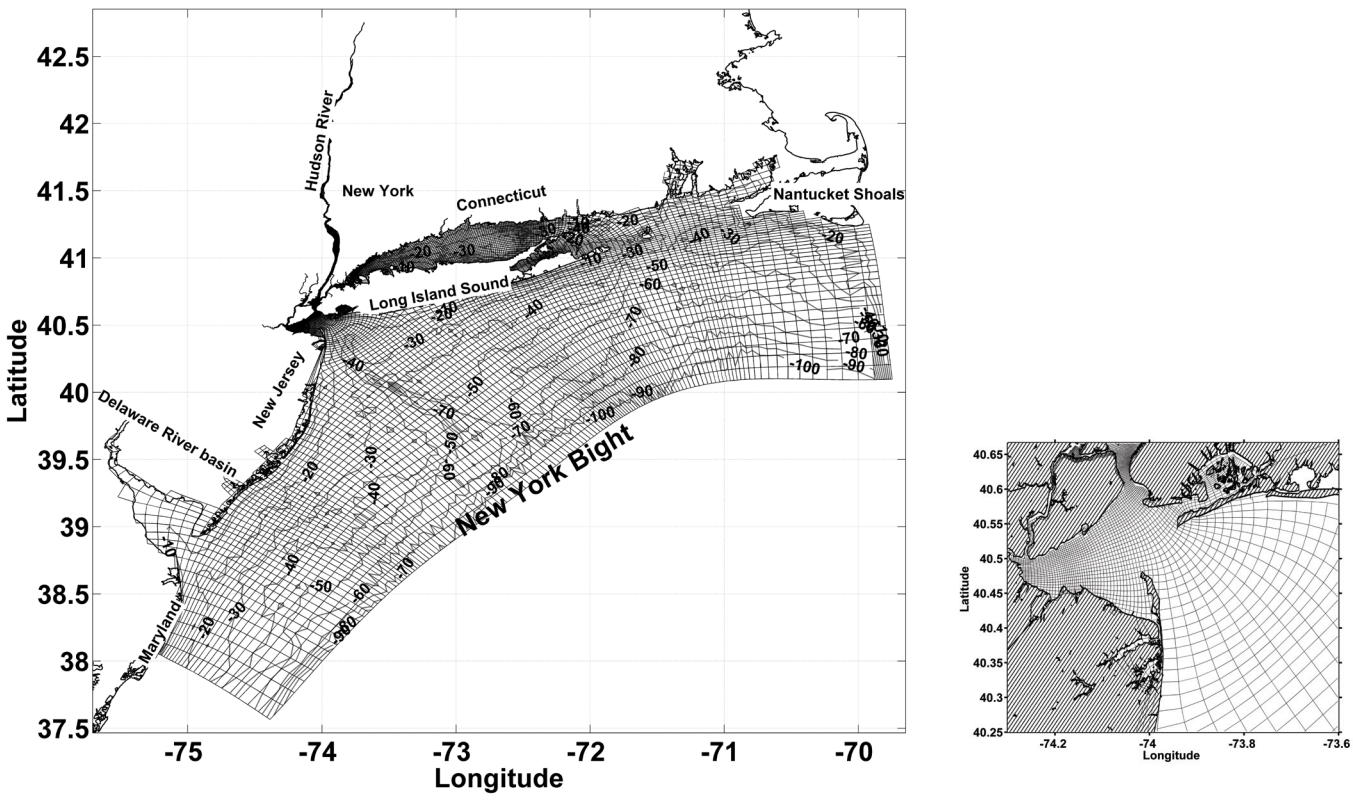

Fig 2: The New York Harbour Observing and Prediction System (NYHOPS) high resolution model grid. The model grid for Raritan Bay and the NYB Apex is zoomed-in and shown in the sub-figure

from Nantucket Island, MA. The model grid resolution varies throughout the domain ranging from approximately 7.5km at the open ocean boundary to less than 50m in several parts of the NY/NJ Harbour Estuary.

The depth of the water column varies from approximately 200m at the open ocean boundary to less than 1m near the shore and in several parts of the NY/NJ Harbour Estuary. The model forcing functions consist of (a) ocean boundary conditions of sea surface elevation, temperature and salinity fields along the open ocean boundary, (b) surface meteorology, and (c) freshwater inflows from rivers, streams, waste-water treatment plants, and point sources from combined sewer overflows and surface run-offs. They have been described in detail.[28]

An extensive hydrodynamic model skill assessment has been conducted recently[28] to quantify the hindcasting and forecasting capabilities of the NYHOPS model. Model results have been compared to *in-situ* observations of water level, currents, temperature, salinity and waves at over 100 locations; collected over a two-year period. The model's ability to describe the hydrodynamic conditions in the extensive area it is employed for is quite good. The average index of agreement[29] for water level is 0.98, for currents 0.87, for water temperature 0.98, for salinity 0.77, and for significant wave height is 0.88. Respective, average root-mean-square (*rms*) errors are: 10cm for water level, 13cm s^{-1} and 9° for currents, 1.4°C for water temperatures, 2.8 psu for salinities, and 32cm for significant wave heights. Additional comparisons of the NYHOPS sea surface temperature predictions against satellite data also show good agreement in the coastal ocean.[30]

HF RADAR DATA ASSIMILATION SCHEME

The present work employs a nudging assimilation scheme to assimilate HF radar data into the NYHOPS model. In the nudging or Newtonian damping scheme, a forcing term is added to the dynamic model which drives the model toward the observations. The rate of nudging must be small and should have a smooth variation with respect to spatial and temporal fields of the ocean state variables as described next.

Nudging scheme

Following the work of previous papers,[31,32,33,34] a nudging term is introduced into the equation of motion as:

$$\frac{\partial U}{\partial t} = \left(physics\right) - \lambda * \left(U - U^{o}\right) \qquad (1)$$

where U represents the model velocity, U^{o} represents the observed velocity, λ represents the nudging parameter, and *(physics)* includes Coriolis, pressure gradients, vertical divergence of shear stress, non-linear advection, and other terms like horizontal and vertical mixing. The velocity U can be either the *u (east-west)* or *v (north-south)* velocity components. The nudging parameter (λ) used in the present study was designed with an exponential spatial and temporal scale dependence. The empirical equation of the nudging parameter (λ) can be represented as:

$$\lambda_{(i,j,k)} = \left[\frac{1}{t_a}\right] * e^{\left[\frac{-r^2}{R_n^2}\right]} * e^{\left[\frac{-(t-t^0)}{t_d}\right]} * e^{\left[\frac{z}{z_d}\right]} \qquad (2)$$

where r is the distance between model grid point and the observed data location, $t - t^0$ is the difference between assimilation and observation time, t_a is the assimilation timescale which determines the strength of the nudging parameter (λ), t_d is the damping time-scale for the nudging term, Rn^2 is the length-scale, $e^{\left[\frac{z}{z_d}\right]}$ is the exponential decay parameter which controls the depth of influence of the nudging parameter (z = 0, at the mean sea-surface, and z_d is the depth of influence).

The method generates sources and sinks near the observational locations. Model dynamics are affected by these 'forces' and the data are imparted to neighbouring (three-dimensional) grid points. The nudging assimilation method is a rough approximation of a standard Optimal Interpolation (OI) scheme, in which the gain matrix *[K]* is analytically specified, rather than deriving by minimising the square of the analysis error covariances.[35]

The present study assimilates HF radar total surface currents which were obtained by combining radial vector fields using the method of least squares[18] with respect to the NYHOPS model horizontal grid. Since HF radar observations were collocated with the NYHOPS model grid point and were linearly interpolated to model time-step between successive observation records, the nudging parameter (λ) can be approximated as

$\lambda_{(i,j,k)} = \left[\frac{1}{t_a}\right] * e^{\left[\frac{z}{z_d}\right]}$, where $e^{\left[\frac{-r^2}{R_n^2}\right]} = 1$, when the model grid point (*i, j, k*) and the observation location remains the same, and $e^{\left[\frac{-(t-t^0)}{t_d}\right]} = 1$, when there is zero time-lag between model and data. The nudging parameter $\lambda(i,j,k)$ = 0, at all other model grid points with no HF radar observations.

The forcing term introduced by the nudging scheme corresponds to the misfit between observed and modelled velocities, scaled by a damping factor (nudging parameter λ, Equation (2)). The nudging parameter attenuates the noisy sources and sinks introduced by the model-data surface velocity misfits.

This nudging scheme for assimilating surface currents was initially applied to an idealised estuary with a long straight channel and a curved configuration.[36] The ocean model was forced with realistic estuarine conditions of river discharge, tidal variation, and density stratification. More insight was obtained about the three-dimensional modifications to current, temperature and salinity fields due to assimilation of synthetic surface currents. The effect of surface current assimilation on the circulation and density stratification for the idealised model experiments suggested there was a need to quality check the magnitude and direction of HF radar-derived surface currents prior to assimilating into the NYHOPS model.

A series of preliminary experimental runs assimilating HF radar surface currents into the NYHOPS model using this nudging scheme were performed. Satisfactory results were obtained using an assimilation time-scale t_a of 1800 seconds, which maintained smooth variation of the misfit perturbations, and the depth of influence z_d of 2.0m, which restricted the assimilation to near-surface layers.

ASSIMILATION RESULTS

The focus of this study is to understand the NYHOPS model performance with respect to model hindcast (defined as the daily model solutions from −24h to 0h) and daily forecast (ie, daily model solutions from 0h to 24) by assimilating HF radar surface currents. Surface currents measured using standard-range HF radar network covering Raritan Bay and the NYB Apex were assimilated into the NYHOPS model for a period of 40 days from 24 February 2007 to 4 April 2007 (referred to 'assimilation period' hereafter) using the nudging assimilation scheme described above. The preceding 24h series of HF radar total surface current maps (obtained at 30 min intervals) were assimilated into the NYHOPS model on daily forecast basis.

Skill metrics

The effectiveness of DA was evaluated by statistically comparing both non-assimilated ('reference') model and assimilated model solutions with *in-situ* observations, which are not used in the assimilation. The DA skill score (DA_{skill}) was based on mean-square-error (*mse*),[37,38] which can be defined as:

$$DA_{skill} = 1 - \frac{mse_a}{mse_r} \tag{3}$$

where mse_r is the mean-square-error of the difference between non-assimilated model solution and observations, and mse_a is the mean-square-error of the difference between assimilated model solution and observations. The DA_{skill} can be defined as a reduction of the *mse* due to assimilation with respect to a non-assimilated model. A positive DA_{skill} (0 ~ 1) represents an improvement in the model performance by assimilation.

A complex vector correlation between model velocities and *in-situ* observations were also computed. Specifically, it has been shown[39] that the magnitude (ρ) and phase (θ) of complex (vector) correlation coefficient ($\rho\, e^{(iO)}$) between any two vector series $w_1(t) = u_1(t) + i\, v_1(t)$, and $w_2(t) = u_2(t) + i\, v_2(t)$ can be estimated in terms of:

$$p = \sqrt{Re^2 + Im^2}, \tag{4}$$

where

$$Re = \frac{\langle u_1 u_2 + v_1 v_2 \rangle}{\langle u_1^2 + v_1^2 \rangle^{1/2} \langle u_2^2 + v_2^2 \rangle^{1/2}} \tag{5}$$

$$Im = \frac{\langle u_1 v_2 - u_2 v_1 \rangle}{\langle u_1^2 + v_1^2 \rangle^{1/2} \langle u_2^2 + v_2^2 \rangle^{1/2}} \tag{6}$$

$$\theta = \tan^{-1} \frac{\langle u_1 v_2 - u_2 v_1 \rangle}{\langle u_1 u_2 + v_1 v_2 \rangle} \tag{7}$$

The magnitude (ρ) represents the overall measure of correlation (< 1.0 by Schwartz inequality) which is independent of any co-ordinate system. The phase angle (θ) represents the average veering between the two vector series, where the phase angle is meaningful only if the magnitude of the correlation is high. The combined set of ($\rho \sim 1$) and ($\theta \sim 0$) denotes an excellent comparison between the two vector series.

The DA_{skill} and vector correlations with respect to three-dimensional currents were computed by comparing model currents with ADCP observations at stations M1 and M2 (see Fig 1) for the assimilation period. The DA_{skill} with respect to three-dimensional temperature (*T*) and salinity (*S*) were obtained by comparing non-assimilated and assimilated model *T* and *S* profiles with glider data from trajectories G1 and G2 (Fig 1) for March 2007. The DA_{skill} were also assessed with respect to fixed-sensor Temperature (*T*) observations for the assimilation period. The DA_{skill} metrics were computed for the NYHOPS model hindcast as well as the first day forecast.

Surface current modifications

HF radar surface current data were nudged into the NYHOPS model in the model hindcast cycle (−24h to 0h) at a temporal resolution of 30 min. The model surface currents (*u* and *v* components) were adjusted using the misfit between modelled currents and HF radar currents, weighted by the nudging parameter (λ). In order to analyse the surface current modifications introduced by the assimilation and to assess the mismatch between HF radar data and modelled currents, HF

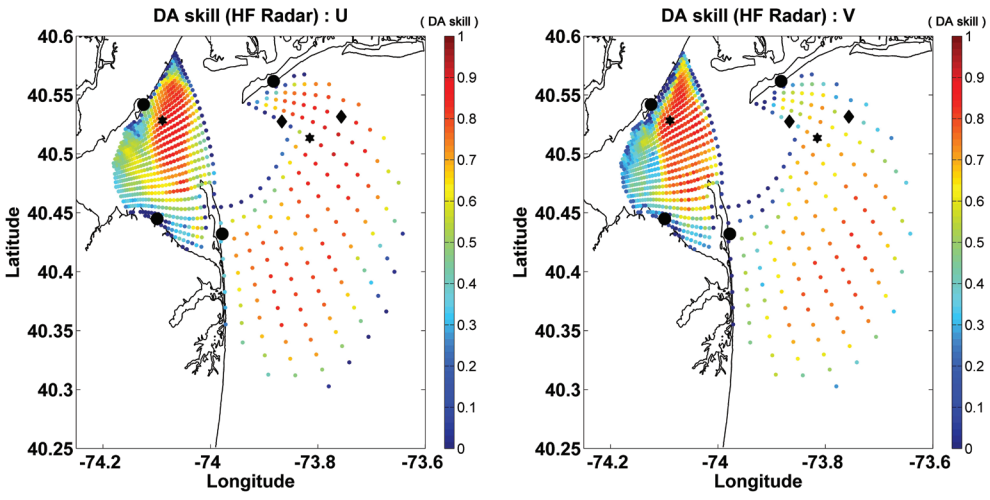

Fig 3: Spatial distribution of DA_{skill} between (non-assimilated and assimilated) model hindcast (daily model solutions from −24h to 0h) and HF radar data for the *u* (left panel) and *v* (right panel) currents. The black '✱' indicates the locations of time-series comparison between HF radar data and NYHOPS (non-assimilated and assimilated) model solution, black '♦' indicates ADCP locations (M1 and M2), and black circles indicate HF radar stations

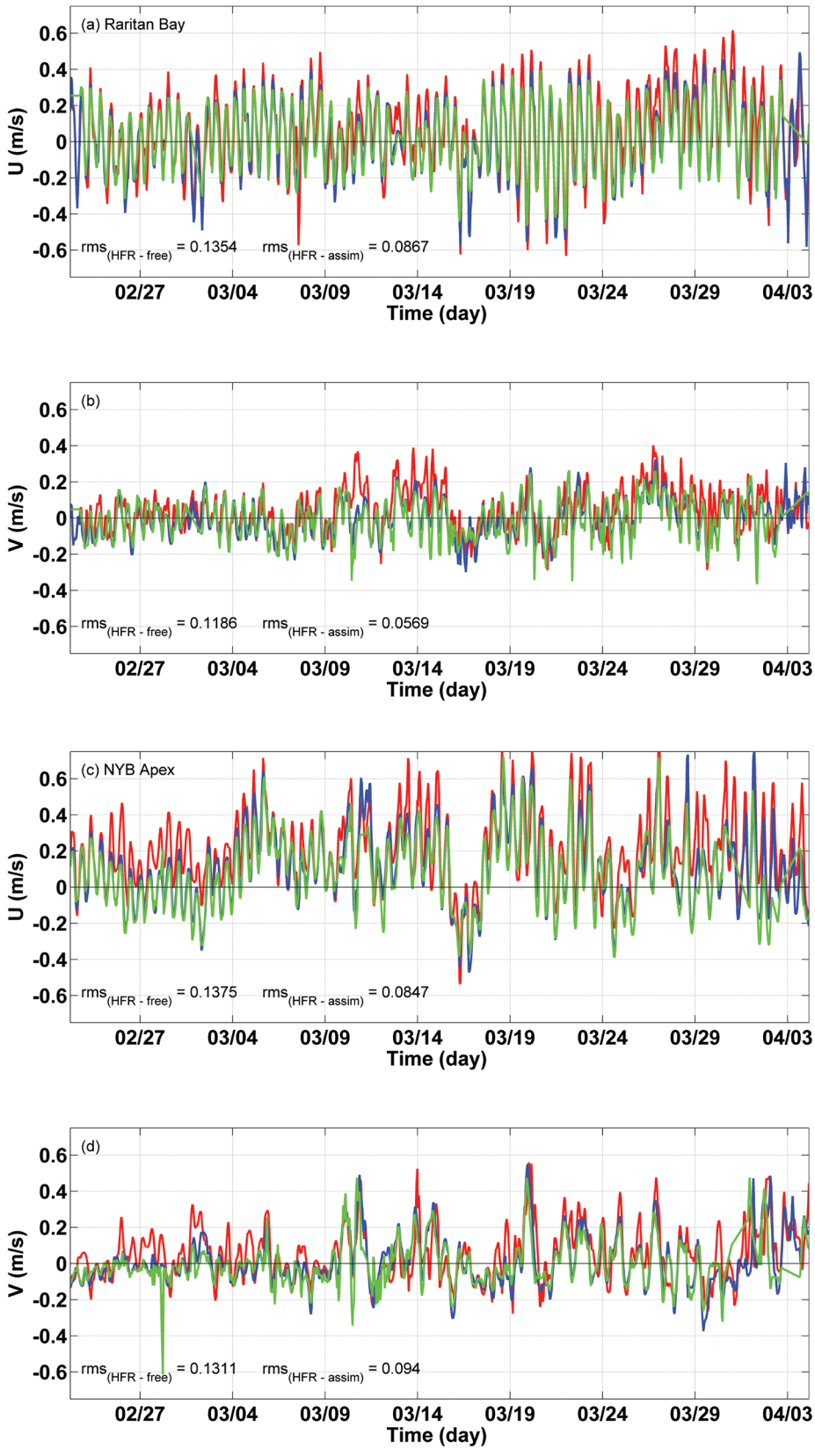

Fig 4: Time-series comparison for the *u* & *v* components of HF radar currents and NYHOPS (non-assimilated and assimilated) model hindcast currents in the Raritan Bay and the NYB Apex (Fig 3 for location) for the assimilation period. Top panels (a) & (b) show hourly HF radar current and model current comparison for Raritan Bay for *u* & *v* components respectively, and bottom panels (c) & (d) show hourly HF radar current and model current comparison for the NYB Apex for *u* & *v* components respectively. Green line indicates HF radar currents, red line indicates non-assimilated (reference) model currents, and blue line indicates assimilated model currents

radar surface currents were compared with non-assimilated and assimilated NYHOPS model near-surface currents for daily model hindcast cycle (–24h to 0h) throughout the assimilation period. The misfit between model currents and HF radar data at every data point of the HF radar footprint were statistically analysed by computing the DA_{skill} (Equation (3)) for both *u* and *v* components (Fig 3).

The DA_{skill} for the Raritan Bay and the NYB Apex in Fig 3 is greater than 0.7 for both *u* and *v* currents, whereas the DA_{skill} degrades and shows a minimum along the periphery of the HF radar data footprint. In order to understand the temporal evolution of the surface currents, the model surface currents and HF radar currents were compared at two locations (marked by black '*' in Fig 3), one in Raritan Bay and the other in the NYB Apex.

The model/observation time-series comparison for *u* and *v* currents for Raritan Bay (Figs 4a & 4b) shows predominant *u* component with a magnitude of ~ 0.5m s^{-1} and *v* component ~ 0.1m s^{-1}. This time-series comparison shows a reasonable agreement between HF radar and assimilated model currents for the predominant *u* component than for the *v* component. The time-series comparison for *u* and *v* currents for the NYB Apex (Figs 4c & 4d) also shows a good agreement between assimilated model currents and HF radar data for both *u* and *v* components. The root-mean-square-error (*rmse*) of the difference between HF radar currents and model currents, labelled in Fig 4, shows considerable reduction in the *rmse* due to assimilation. The time-series comparison at these two locations demonstrate that the nudging term, represented by the model-data misfit and weighted by the nudging parameter (λ), introduced into the model momentum equations behaves as expected, adjusting the model currents toward HF radar observations.

Data assimilation skill for velocities based on ADCP observations

The DA_{skill} for the *u* and *v* component with respect to ADCP data (at stations M1 and M2) for model hindcasts and forecasts are shown in Fig 5. The hindcast DA_{skill} with respect to M1 ADCP data (Fig 5a) shows a positive skill throughout the water column for both *u* and *v* components. A maximum skill of +24% was achieved for the predominant *u* component at near-surface layers, whereas *v* component shows a maximum skill of +20% at sub-surface layers. The hindcast DA_{skill} with respect to M2 ADCP data is shown in Fig 5b, where M2 ADCP failed to provide reliable data at near-surface layers (~ 6.2m from the surface). Based on M2 ADCP data, a positive skill was achieved at sub-surface layers for both *u* and *v* components with a maximum skill of +48% (+30%) for the *u* (*v*) components, and the skill degrades with increasing depth at near-bottom layers for both *u* and *v* components.

The DA_{skill} with respect to ADCP (M1 and M2) data for model forecasts are shown in Figs 5c & 5d. The forecast DA_{skill} with respect to M1 ADCP data (Fig 5c) shows a positive skill throughout the water column for both *u* and *v* components with a maximum skill of +18% for the predominant *u* component at

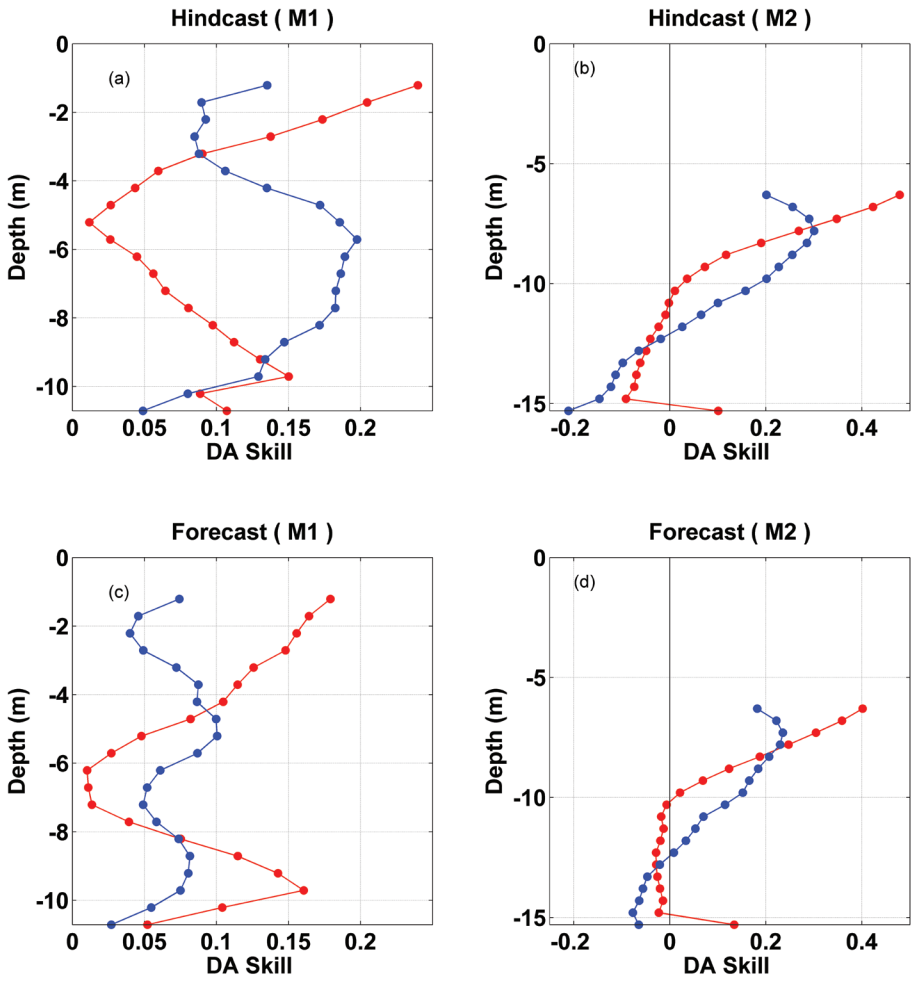

Fig 5: Model hindcast (–24h to 0h) DA_{skill} [top panels (a) & (b)] and first day model forecast (0h to 24h) DA_{skill} [bottom panels (c) & (d)] for the *u* and *v* components with respect to ADCP (M1 and M2) data. Top panels (a) & (b) show the model hindcast DA_{skill} with respect to M1 ADCP data and M2 ADCP data and bottom panels (c) & (d) show the model forecast DA_{skill} with respect to M1 ADCP data and M2 ADCP data. Blue solid line indicates DA_{skill} for *u* component and red solid line indicates DA_{skill} for *v* component

near-surface layers and a maximum skill of +10% for *v* component at sub-surface layers. The forecast DA_{skill} with respect to M2 ADCP data (Fig 5d) also shows a positive skill of +40% (+22%) for the *u*(*v*) components at sub-surface layers.

The model forecast DA_{skill} shows a similar variation along the depth as that of the model hindcasts, but with a decrease in the skill magnitude. This decrease in the forecast DA_{skill} may be due to the fact that HF radar data were assimilated only into the NYHOPS model hindcast cycle. The present study uses a weaker nudging parameter (λ) by defining an assimilation timescale (t_a) of 1800 seconds in order to ensure a smaller rate of nudging and smooth variation of the ocean state parameters in space and time. This weaker nudging parameter down-weights the impact of noisy sources and sinks ('shocks') introduced by the model-data surface current misfits. Once the model completes the hindcast cycle and starts forecasting, HF radar data is no longer nudged into the model momentum equations, and the impact of the model state adjustments imparted during the model hindcast cycle diminishes gradually over the forecasting time.

The vector correlation (ρ, θ) between model currents and the ADCP data for model hindcasts and forecasts are shown in Fig 6. The complex correlation values between (non-assimilated and assimilated) model hindcast currents and ADCP data (Figs 6a & 6b) shows an overall increase in the magnitude of the complex correlation (ρ) and a decrease in the average veering angle (θ) between model currents and ADCP data by surface current assimilation. This represents an improvement in the model performance by assimilation. The vector correlation statistics (ρ, θ) between (non-assimilated and assimilated) model forecast currents and the ADCP data are shown in Figs 6c & 6d, which also show a similar vertical structure along the depth as that of the model indcasts, but with a less pronounced effect of surface current assimilation.

Based on model-ADCP data comparison, DA_{skill} shows improved model performance at the near-surface and the sub-surface layers for both model hindcasts and forecasts. HF radar surface current assimilation increases the magnitude of the complex correlation (ρ) and decreases the average veering

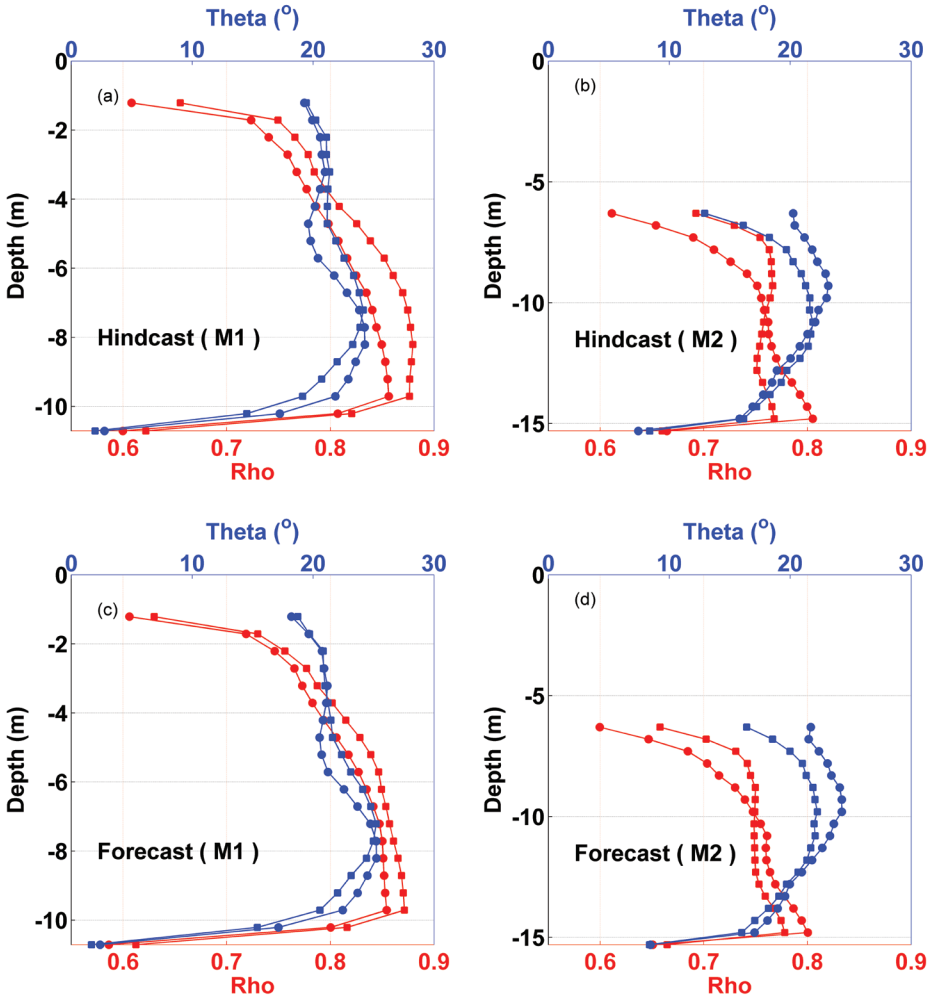

Fig 6: Model hindcast (–24h to 0h) vector correlation (ρ and θ) [top panels (a) & (b)] and first day model forecast (0h to 24h) vector correlation (ρ and θ) [bottom panels (c) & (d)] with respect to ADCP (M1 and M2) data. Top panels (a) & (b) show the vector correlation (ρ and θ) for (non-assimilated and assimilated) model hindcast with respect to M1 ADCP data and M2 ADCP data, and bottom panels (c) & (d) show the vector correlation (ρ and θ) for the (non assimilated and assimilated) model forecasts with respect to M1 ADCP data and M2 ADCP data. In each plot, top x-axis represent θ (blue solid line) and bottom x-axis represent ρ (red solid line). Lines marked with '•' indicate non-assimilated (reference) model, while '□' indicates assimilated model

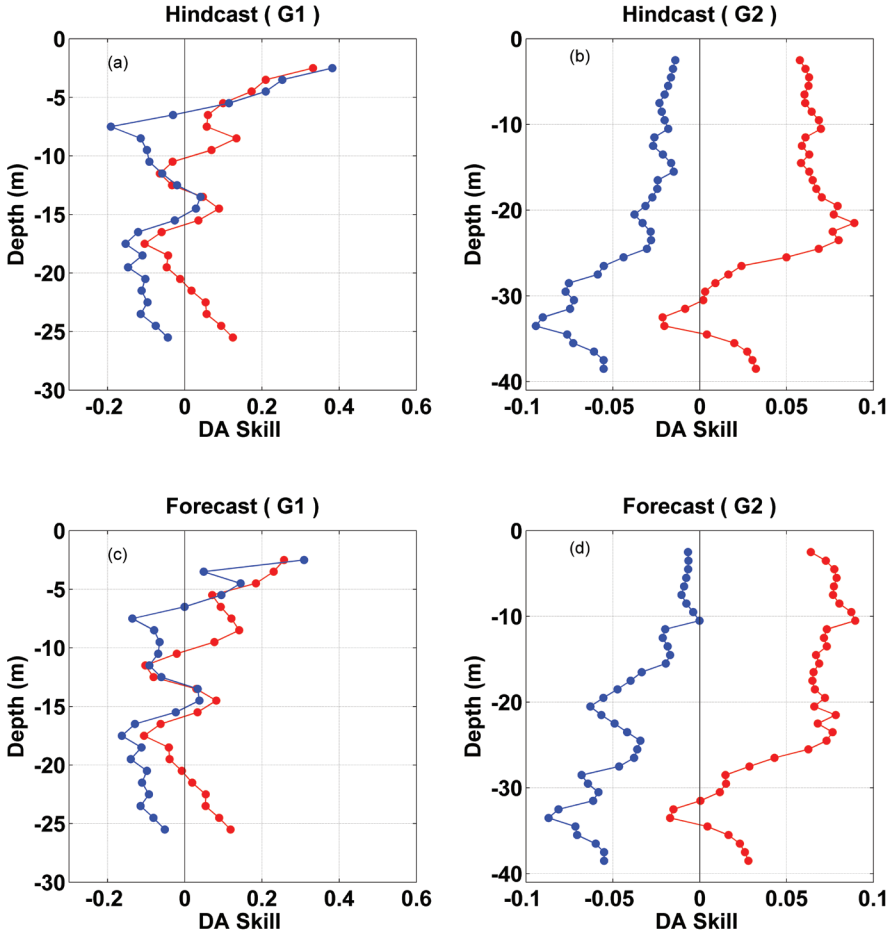

Fig 7: Model hindcast (–24h to 0h) DA_{skill} [top panels (a) & (b)] with respect to G1 glider data for the inner-NJ shelf region (a) and with respect to G2 glider data for the mid-NJ shelf region (b). Model forecast (0h to 24h) DA_{skill} [bottom panels (c) & (d)] with respect to G1 glider data for the inner-NJ shelf region (c) and with respect to G2 glider data for the mid-NJ shelf region (d). Red solid line indicates DA_{skill} for *T* and blue solid line indicate DA_{skill} for *S*

angle (θ) between model currents and ADCP data, for both model hindcasts and forecasts, showing an enhancement in the model performance.

Temperature and salinity assimilation skill based on glider observations

The effectiveness of DA with respect to three-dimensional Temperature (*T*) and Salinity (*S*) distributions in the regions outside the assimilation domain was studied by comparing non-assimilated and assimilated model *T* and *S* profiles with glider (G1 and G2 trajectories, sub-figure in Fig 1) *T* and *S* data. The improvements in the model performance by HF radar DA were assessed by computing the DA_{skill} with respect to three-dimensional *T* and *S* fields. The NYHOPS model solutions for *T* and *S*, for both model hindcasts as well as forecasts, were linearly interpolated in time and space to glider profiles. The DA_{skill} is based on *mse* of the difference between non-assimilated and assimilated model *T* and *S* profiles and glider profiles. The DA_{skill} (Equation (3)) for *T* and *S* were computed as a function of the depth for the regions of inner-NJ shelf (0 ~ 30m) and mid-NJ shelf (30 ~ 90m) for the period of glider flights (March 2007). The model hindcast DA_{skill} for *T* and *S* fields in the inner-NJ shelf region with respect to G1 glider data is shown in Fig 7a. In the inner-NJ shelf region, DA shows reasonable improvement in hindcasting *T* and *S* at the near-surface layers, showing a DA_{skill} of 33% (38%) for *T* (*S*). The model hindcast DA_{skill} for *T* and *S* fields in the mid-NJ shelf region with respect to G2 glider data is shown in Fig 7b. Surface current assimilation shows only moderate improvement in hindcasting *T* in the mid-NJ shelf region. The DA_{skill} based on glider data (G1 and G2) for model forecasts are shown in Figs 7c & 7d, which show a similar variation along the depth as that of the model hindcasts, with the near-surface layers showing a forecast DA_{skill} of 25% (30%) for *T* (*S*) for the inner-NJ shelf region. The forecast DA_{skill} based on glider data (G1 and G2) shows a decrease in the skill magnitude compared to model hindcast, which is consistent with other assimilation skills discussed above.

Data assimilation skill for temperature based on fixed-sensor observations

The non-assimilated and assimilated model *T* were compared with *in-situ T* observations from the fixed-sensors. The computed DA_{skill} with respect to *T* observations were tabulated, shown in Table 1. The assimilated model *T* showed a better comparison with *in-situ* observations than non-assimilated model, showing an improved model performance by surface current assimilation for both model hindcasts and forecasts. The DA_{skill} for the model forecasts were similar to that for the

Location	Station Name	Agency	Parameter	Depth	DA_{skill} Hindcast	DA_{skill} Forecast
The Battery, NJ	BATN6	NOS	Temperature	Surface	+11%	+12%
Sandy Hook, NJ	SDHN4	NOS	Temperature	Surface	+34%	+36%
Belford, NJ	STBLD4	SIT	Temperature	Bottom	+12%	+11%
ADCP mooring: 1	M1	RU	Temperature	Bottom	+5%	+5%
ADCP mooring: 2	M2	RU	Temperature	Bottom	+11%	+10%

Table 1: Data assimilation skill for the NYHOPS model (comparison with fixed-sensor temperature observations)

model hindcasts for all the stations and shows an increased skill based on the near-surface *T* observations than for the near-bottom *T* observations.

SUMMARY AND DISCUSSION

A nudging scheme is implemented to assimilate HF radar surface currents into the NYHOPS model. HF radar total surface currents were assimilated into the NYHOPS model for a period of 40 days (24 Feb 2007–4 April 2007). The impact of DA in the model performance was evaluated by computing the DA_{skill}, and a positive DA_{skill} (0 ~ 1) represents an improvement in the model performance by assimilation. The DA_{skill} were based on the *mse* of the difference between non-assimilated and assimilated model solutions and *in-situ* observations of three-dimensional (*u*, *v*) currents, temperature (*T*), and salinity (*S*), which are not used in the assimilation. The present work focused on the NYHOPS model performance in hindcasting (daily model solutions from −24h to 0h) and forecasting (first day forecast: daily model solutions from 0h to 24h) the ocean state by assimilating HF radar surface currents. The DA_{skill} was computed by comparing model solutions with ADCP (at stations M1 and M2) observations for three-dimensional (*u*, *v*) currents, glider (G1 and G2 trajectories) observations for three-dimensional *T* and *S*, and fixed-sensor *T* observations.

The DA_{skill} analysis based on three-dimensional currents obtained from ADCPs (M1 and M2) showed a reasonable improvement in the NYHOPS model performance by surface current assimilation for both model hindcasts and forecasts. Comparison with M1 ADCP data showed a positive DA_{skill} throughout the water column for both *u* and *v* components, for the NYHOPS model hindcasts as well as forecasts. Model skill metrics based on M1 ADCP data for the near-surface layers in the inner-NJ shelf region showed a hindcast DA_{skill} of 24% (14%) and forecast DA_{skill} of 18% (7%) for three-dimensional *u* (*v*) currents. Comparison with M2 ADCP data showed positive DA_{skill} for the sub-surface layers for both *u* and *v* components, for the NYHOPS model hindcasts as well as forecasts. Based on M2 ADCP data a hindcast DA_{skill} of 48% (30%) and forecast DA_{skill} of 40% (18%) were achieved for three-dimensional currents *u* (*v*) at the sub-surface layers, and the skill degrades with increasing depth at near-bottom layers. The vector correlation statistics between model currents and ADCP data showed an overall increase in the magnitude of the complex correlation (ρ) and a decrease in the average veering angle (θ) between model currents and ADCP currents, showing an improved model performance by surface current assimilation for both model hindcasts as well as forecasts.

The modifications to three-dimensional *T* and *S* fields due to assimilation were studied by comparing non-assimilated and assimilated model *T* and *S* solutions with glider (G1 and G2) *T* and *S* profiles, for model hindcasts as well as forecasts. A positive DA_{skill} were achieved for *T* and *S* for the near-surface layers in inner-NJ shelf region for both model hindcasts and forecasts, showing a hindcast DA_{skill} of 33% (38%) and forecast DA_{skill} of 25% (30%) for three-dimensional temperature (salinity). The glider flights falls outside the assimilation domain and the improvement in the model performance suggests the influence of HF radar DA beyond the assimilation domain via model dynamics. The DA_{skill} metrics for the mid-NJ shelf region showed no considerable improvement in the model performance. This low DA_{skill} score in the mid-NJ shelf regions might be due to the influence of offshore climatological open boundary conditions. The coarser resolution (~ 7.5km) of the model curvilinear grid along the offshore mid-NJ shelf region may also influence the poor DA_{skill} with respect to glider data. The DA_{skill} were also computed with respect to fixed-sensor (*T*) observations. HF radar assimilation showed positive DA_{skill} at all the locations with pronounced improvement with respect to near-surface *T* for both the model hindcasts and forecasts than for the near-bottom *T*.

The nudging scheme is robust and efficient for the HF radar DA into the NYHOPS operational forecast model, resolving the tidal frequency variability. The assimilation system is capable of importing in the observations and provides improved hindcasts and forecasts for the study domain with the lowest computing cost of application. Future work will focus on assimilating HF radar data, drifter data, and satellite Sea Surface Temperature (SST) data covering the Mid-Atlantic Bight and the New York Bight into the NYHOPS operational forecast model.

ACKNOWLEDGEMENTS

This work was supported by grants from Office of Naval Research (ONR) (Grant: N00014-06-1-1027) and National Oceanic and Atmospheric Administration (NOAA) (Grant: NA17RJ1231). The authors thank Wendell Brown for his valuable insights and constructive reviews, and also thank Scott Glenn, Josh Kohut and Hugh Roarty at the Coastal Ocean Observation Laboratory, Rutgers University, for helpful discussions and for providing *in-situ* data for model skill analysis. The authors also acknowledge Richard Hires,

Nickitas Georgas and Dov Kruger at the Center for Maritime Systems, Stevens Institute of Technology. Special thanks to Jack Harlan (NOAA, IOOS) for supporting the temporary HF radar station at Bay Shore, NJ.

REFERENCES

1. Anderson D, Sheinbaum J and Haines K. 1996. *Data assimilation in ocean models, Reports on*. Progress in Physics, *59*, 1209–1266.

2. Lewis J, Shulman I and Blumberg A. 1998. *Assimilation of CODAR observations into ocean models*. Continental Shelf Research, 18, 541–559.

3. Breivik Ø and Sætra Ø. 2001. *Real time assimilation of HF radar currents into a coastal ocean model*. Journal of marine systems, 28(3–4), 161–182.

4. Oke P, Allen J, Miller R, Egbert G and Kosro P. 2002b. *Assimilation of surface velocity data into a primitive equation coastal ocean model*. J. Geophys. Res, 107(C9).

5. Bennett AF. 2002. Inverse modelling of the ocean and the atmosphere. Cambridge Univ. Press, New York.

6. Kurapov A, Egbert G, Allen J, Miller R, Erofeeva S and Kosro P. 2003. *The M2 internal tide off Oregon: Inferences from data assimilation*. Journal of Physical Oceanography, 33(8), 1733–1757.

7. Paduan J and Shulman I. 2004. *HF radar data assimilation in the Monterey Bay area*. Journal of Geophysical Research-Oceans, 109(C7), C07S09.

8. Wilkin J, Arango H, Haidvogel D, Lichtenwalner C, Glenn S and Hedstrom K. 2005. *A regional ocean modelling system for the long-term ecosystem observatory*. J. Geophys. Res, 110, C06S91.

9. Barth A, Alvera-Azcárate A and Weisberg R. 2008. *Assimilation of high-frequency radar currents in a nested model of the West Florida Shelf*. Journal of geophysical research. C, Oceans, 113(c8), 1-C08,033.

10. Li Z, Chao Y, McWilliams J and Ide K. 2008. A three-dimensional variational data assimilation scheme for the Regional Ocean Modelling System: Implementation and basic experiments. *Journal of Geophysical Research*, *113*, C05,002.

11. Hoteit I, Cornuelle B, Kim S, Forget G, Kohl A and Terrill E. 2009. *Assessing 4D-VAR for dynamical mapping of coastal high-frequency radar in San Diego*. Dynamics of Atmospheres and Oceans, 48(1–3), 175–197.

12. Shulman I and Paduan J. 2009. *Assimilation of HF radar-derived radials and total currents in the Monterey Bay area*. Deep-Sea Research Part II, 56(3–5), 149–160.

13. Barrick D, Evans M and Weber B. 1977. *Ocean surface currents mapped by radar*. Science, 198(4313), 138.

14. Paduan J and Graber H. 1997. *Introduction to high-frequency radar: Reality and myth*. Oceanography, 10(4), 36–39.

15. Paduan J and Rosenfeld L. 1996. *Remotely sensed surface currents in Monterey Bay from shore-based HF radar (Coastal Ocean Dynamics Application Radar)*. Journal of geophysical Research, 101(C9), 20,669–20,686.

16. Graber H, Haus B, Chapman R and Shay L. 1997. *HF radar comparisons with moored estimates of current speed and direction: Expected differences and implications*. Journal of geophysical research, 102(C8), 18,749–18,766.

17. Schmidt R. 1986. *Multiple emitter location and signal parameter estimation*. IEEE Transactions on Antennas and Propagation, 34(3), 276–280.

18. Lipa B and Barrick D. 1983. *Least-squares methods for the extraction of surface currents from CODAR crossed-loop data: Application at ARSLOE*. IEEE Journal of Oceanic Engineering, 8(4), 226–253.

19. Stewart R and Joy J. 1974. *HF radio measurements of surface currents*. Deep Sea Research and Oceanographic Abstracts, Vol 21, pp500 1039–1049, Elsevier.

20. Gopalakrishnan G and Blumberg AF. 2011. *Surface currents in Raritan Bay, NJ: Importance of HF radar first-order Doppler settings*. J. Operational Oceanography, Vol 4 No2, pp41–53.

21. Chapman R and Graber H. 1997. *Validation of HF radar measurements*. Oceanography.Washington DC-Oceanography Society, 10, 76–79.

22. Bruno M, Blumberg A andHerrington T. 2006. *The urban ocean observatory - coastal ocean observations and forecasting in the New York Bight*. J. Mar. Sci. Environ, 4, 1–9.

23. Blumberg A and Mellor G. 1987. *A description of a three-dimensional coastal ocean circulation model*. Three-dimensional coastal ocean models, 4, 1–16.

24. Mellor G and Yamada T. 1982. *Development of a turbulence closure model for geophysical fluid problems*. Reviews of Geophysics and Space Physics, 20(4), 851–875.

25. Galperin B, Kantha L, Hassid S and Rosati A. 1988. *A quasi-equilibrium turbulent energy model for geophysical flows*. Journal of the Atmospheric Sciences, 45(1), 55–62.

26. Blumberg A, Galperin B and O'Connor D. 1992. *Modelling vertical structure of open-channel flows*. Journal of Hydraulic Engineering, 118(8), 1119–1134.

27. Smagorinsky J. 1963. *General circulation experiments with the primitive equations*. Monthly weather review, 91(3), 99–164.

28. Georgas N and Blumberg A. 2010. *Establishing confidence in marine forecast systems: The design and skill assessment of the New York Harbour Observation and Prediction System (NY-HOPS) version 3*. Proceedings of the Eleventh International Conference on Estuarine and Coastal Modelling (ECM11), American Society of Civil Engineers.

29. Willmott C. 1981. *On the validation of models*. Physical Geography, 2(2), 184–194.

30. Bhushan S, Blumberg A and Georgas N. 2010. *Comparison of the NYHOPS hydrodynamic model Sea Surface Temperature (SST) predictions with satellite observations in the Hudson River tidal, estuarine, and coastal plume region*. Proceedings of the Eleventh International Conference on Estuarine and Coastal Modelling (ECM11), American Society of Civil Engineers.

31. Fan S, Oey L and Hamilton P. 2004. *Assimilation of drifter and satellite data in a model of the Northeastern Gulf of Mexico*. Continental Shelf Research, 24(9), 1001–1013.

32. Oey L. 2008. *Loop current and deep eddies*. Journal of Physical Oceanography, 38(7), 1426–1449.

33. Lin X., Oey L and Wang D. 2007. *Altimetry and drifter data assimilations of loop current and eddies*. Journal of Geophysical Research (Oceans), 112(C11), 05,046.

34. Chang Y and Oey L. 2010. Eddy and wind-forced heat transports in the Gulf of Mexico. *Journal of Physical Oceanography*.

35. Daley R. 1991. Atmospheric data analysis. Cambridge Atmospheric and Space Science series.

36. Gopalakrishnan G, Blumberg A and Hires R. 2007. *Assimilating surface current data into a model of estuarine and coastal ocean circulation*. Proceedings of the Tenth International Conference on Estuarine and Coastal Modelling (ECM10), American Society of Civil Engineers.

37. Murphy A. 1992. *Climatology, persistence, and their linear combination as standards of reference in skill scores*. Weather and forecasting, 7(4), 692–698.

38. Oke P, Allen J, Miller R, Egbert G, Austin J, Barth J, Boyd T, Kosro P and Levine M. 2002a. *A modelling study of the three-dimensional continental shelf circulation off Oregon. Part I: Model-data comparisons*. Journal of Physical Oceanography, 32(5), 1360–1382.

39. Kundu P. 1976. *Ekman veering observed near the ocean bottom*. Journal of Physical Oceanography, 6(2), 238–242.